JOC Article
pubs.acs.org/joc

Absolute Configuration Assignment of Norcamphor-Derived Furyl Hydroperoxide Using Density Functional Theory Calculations of Optical Rotation and Vibrational Circular Dichroism

Alessandra Lattanzi, Arrigo Scettri, and Riccardo Zanasi*

Dipartimento di Chimica, Università di Salerno, via Ponte don Melillo, 84084 Fisciano (SA), Italy

Frank J. Devlin and Philip J. Stephens*

Department of Chemistry, University of Southern California, Los Angeles, California 90089-0482

rzanasi@unisa.it; pstephen@usc.edu

Received November 19, 2009

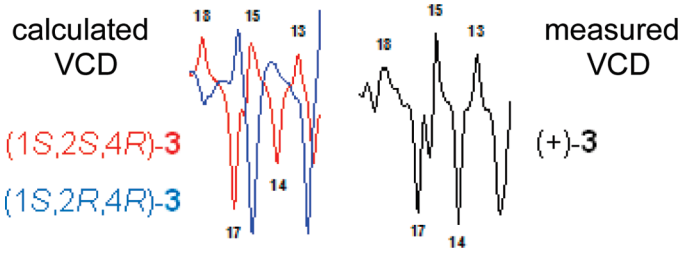

Density functional theory (DFT) calculations of sodium D line specific rotation and of vibrational circular dichroism (VCD) have been used to assign the absolute configuration of a recently prepared (1*S*,4*R*)-norcamphor-derived furyl hydroperoxide, (+)-**3**, introduced as a stereoselective oxidant. Both approaches give the same absolute configuration to the newly generated stereogenic carbon at position 2, i.e., (1*S*,2*S*,4*R*)-(+)-**3**, thus providing a confident assignment in a case made difficult by the large conformational flexibility and the small difference between the computed optical rotations of the two possible diastereoisomers. Although the computed IR absorption spectra of (1*S*,2*S*,4*R*)-**3** and (1*S*,2*R*,4*R*)-**3** are practically indistinguishable, a number of significant differences in the VCD spectra of these two nonmirror-image isomers can be observed, which allows the structural identification of the synthesized compound. This is clearly shown here for the first time.

Introduction

The use of optically pure tertiary alkyl hydroperoxides as stereoselective oxidants has received increasing interest in recent years. However, few examples have appeared[1] because of the lack of general synthetic approaches to these types of compounds in optically pure form and their intrinsic limited chemical stability.[2] These compounds have been obtained by using horseradish peroxidase mediated reductive kinetic resolution of racemic secondary alkyl hydroperoxides[3] or by using compounds from the chiral pool as initial building blocks for their synthesis. The only example of a tertiary enantiopure hydroperoxide TADOOH (Scheme 1),

*To whom correspondence should be addressed. (R.Z.) Tel: +39 089 969590. Fax: +39 089 969603. (P.J.S.) Tel: +1 213 740 4119. Fax: +1 213 740 3972.

(1) (a) Takata, T.; Ando, W. *Bull. Chem. Soc.* **1986**, *59*, 1275. (b) Adam, W.; Korb, M. N. *Tetrahedron: Asymmetry* **1997**, *8*, 1131. (c) Adam, W.; Korb, M. N.; Roschmann, K. J.; Saha-Möller, C. R. *J. Org. Chem.* **1998**, *63*, 3423. (d) Hamann, H.-J.; Höft, E.; Mostowicz, D.; Mishnev, A.; Urbańczyk-Lipkowska, Z.; Chmielewski, M. *Tetrahedron* **1997**, *53*, 185. (e) Mostowicz, D.; Jurczak, M.; Hamann, H.-J.; Höft, E.; Chmielewski, M. *Eur. J. Org. Chem.* **1998**, 2617. (f) Dwyer, C. L.; Gill, C. D.; Ichihara, O.; Taylor, R. J. K. *Synlett* **2000**, 704. (g) Aoki, M.; Seebach, D. *Helv. Chim. Acta* **2001**, *84*, 187. (h) Adam, W.; Alsters, P. L.; Neumann, R.; Saha-Möller, C. R.; Seebach, D.; Zhang, R. *Org. Lett.* **2003**, *5*, 725.

(2) (a) Cekovic, Z.; Green, M. M. *J. Am. Chem. Soc.* **1974**, *96*, 3000. (b) Saussine, L.; Brazi, E.; Robine, A.; Mimoun, H.; Fischer, J.; Weiss, R. *J. Am. Chem. Soc.* **1985**, *107*, 3534.

(3) (a) Adam, W.; Hoch, U.; Saha-Möller, C. R.; Schreier, P. *Angew. Chem, Int. Ed.* **1993**, *32*, 1737. (b) Adam, W.; Hoch, U.; Lazarus, M.; Saha-Möller, C. R.; Schreier, P. *J. Am. Chem. Soc.* **1996**, *117*, 11898.

DOI: 10.1021/jo902472b Published on Web 03/04/2010

SCHEME 1. Optically Pure Tertiary Alkyl Hydroperoxides and Alcohol

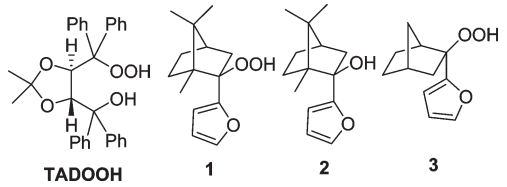

synthesized from (−)-TADDOL, proved to be the best reagent in various stereoselective oxidative processes,[1g] thus confirming that the highest level of asymmetric induction can be achieved with the most stable tertiary hydroperoxides.[4]

On the basis of our interest in metal-catalyzed asymmetric oxidations, we have recently developed a simple two-step synthesis of a tertiary furyl hydroperoxide **1** (Scheme 1) employing (*R*)-camphor as a readily available starting compound.[5]

Unlike TADOOH, where the same stereogenic carbon centers are present in the (−)-TADDOL alcohol used as the chiral source for the synthesis, in our case, the carbon bearing the hydroperoxyl group is a newly generated stereogenic center in **1** whose absolute configuration (AC) was determined by NOESY experiments on the corresponding alcohol **2**, obtained after reduction of oxidant **1**.[6] Absolute configurations of secondary alkyl hydroperoxides have been previously determined after reduction of the hydroperoxide to the corresponding alcohol, which was properly derivatized and then analyzed by exciton-coupled circular dichroism.[7] No direct determinations of the absolute configurations of enantiopure tertiary alkyl hydroperoxides have been reported up to now by experimental methods. Using a theoretical method, we have proposed a straightforward determination of the absolute configurations of **1** and **2** by time-dependent density functional theory (TDDFT) calculations of the optical rotation (OR).[8]

With the hope of improving the reactivity of the sterically crowded oxidant **1** and to enlarge the access to a variety of tertiary enantiopure hydroperoxides of this type, we have recently prepared a less hindered hydroperoxide **3** (see Scheme 2).[9]

Furyl alcohol **5** was efficiently obtained via furyllithium addition to (+)-norcamphor **4**,[10] and according to the literature,[11] the formation of the *endo* diastereoisomer of **5** would have occurred thanks to the attack of the organometallic reagent exclusively from the less sterically demanding *exo*-face of the ketone. The hydroperoxidation of alcohol **5** furnished exclusively a single diastereoisomer of hydroperoxide **3** in high yield, having a positive optical rotation in both $CHCl_3$ (+36.4, $c = 1.00$) and hexane (+36.9, $c = 1.00$).

On the grounds of literature precedents concerning the reactivity of 2-substituted norbornyl cation intermediates in nucleophilic substitutions,[5a,12] epimerization at carbon 2 of the bicyclic framework of alcohol **5** is expected to occur during the oxidation. Actually, the inverted absolute configuration at carbon 2 of **3** with respect to **5** was indirectly established after the reduction to alcohol by comparison of

(4) (a) Rossiter, B. E. In *Asymmetric Synthesis*; Morrison, J. D., Ed.; Academic Press: New York, 1985; Vol. 5, p 193. (b) Finn, M. G.; Sharpless, K. B. In *Asymmetric Synthesis*; Morrison, J. D., Ed.; Academic Press: New York, 1985; Vol. 5, pp 347.

(5) (a) Lattanzi, A.; Iannece, P.; Vicinanza, A.; Scettri, A. *Chem. Commun.* **2003**, 1440. (b) Lattanzi, A.; Scettri, A. *Curr. Org. Chem.* **2004**, *8*, 607.

(6) The reduction process is known to proceed with retention of configuration; see: Denney, D. B.; Goddyear, W. F.; Goldstein, B. *J. Am. Chem. Soc.* **1960**, *82*, 1393.

(7) (a) Hoch, U.; Humpf, H.-U.; Schreier, P.; Saha-Möller, C. R.; Adam, W. *Chirality* **1997**, *9*, 69. (b) Adam, W.; Humpf, H.-U.; Korb, M. N.; Schreier, P. *Tetrahedron: Asymmetry* **1997**, *8*, 3555.

(8) Lattanzi, A.; Viglione, R. G.; Scettri, A.; Zanasi, R. *J. Phys. Chem. A* **2004**, *108*, 10753.

(9) Lattanzi, A.; Iannece, P.; Scettri, A. *Tetrahedron: Asymmetry* **2004**, *15*, 1779.

(10) (1*S*,4*R*)-Norcamphor was obtained by oxidation of commercial (+)-*endo*-2-norborneol; see: Kawamura, M.; Ogasawara, K. *Tetrahedron Lett.* **1995**, *36*, 3369.

(11) Olah, G. A.; Berrier, A. L.; Surya Prakash, G. K. *J. Org. Chem.* **1982**, *47*, 3903.

(12) (a) Ikegami, S.; Vander Jagt, D. L.; Brown, H. C. *J. Am. Chem. Soc.* **1968**, *90*, 7124. (b) Goering, H. L.; Brown, H. C.; Schewene, C. B. *J. Am. Chem. Soc.* **1968**, *90*, 6214. (c) Lenoir, D.; Apeloig, Y.; Arad, D.; Schleyer, P. v. R. *J. Org. Chem.* **1988**, *53*, 661. (d) Brown, H. C.; Ravindranathan, M.; Gundu Rao, C.; Chloupek, F. J.; Rei, M.-H. *J. Org. Chem.* **1978**, *43*, 3667. (e) Grob, C. A.; von Sprecher, G.; Waldner, A. *Helv. Chim. Acta* **1983**, *66*, 2656.

(13) (a) Cheeseman, J. R.; Frisch, M. J.; Devlin, F. J.; Stephens, P. J. *J. Phys. Chem. A* **2000**, *104*, 1039. (b) Stephens, P. J.; Devlin, F. J.; Cheeseman, J. R.; Frisch, M. J. *J. Phys. Chem. A* **2001**, *105*, 5356. (c) Grimme, S. *Chem. Phys. Lett.* **2001**, *339*, 380. (d) Ruud, K.; Helgaker, T. *Chem. Phys. Lett.* **2002**, *352*, 533. (e) Mennucci, B.; Tomasi, J.; Cammi, R.; Cheeseman, J. R.; Frisch, M. J.; Devlin, F. J.; Gabriel, S.; Stephens, P. J. *J. Phys. Chem. A* **2002**, *106*, 6102. (f) Autschbach, J.; Patchkovskii, S.; Ziegler, T.; van Gisbergen, S. J. A.; Baerends, E. J. *J. Chem. Phys.* **2002**, *117*, 581. (g) Grimme, S.; Furche, F.; Ahlrichs, R. *Chem. Phys. Lett.* **2002**, *361*, 321. (h) Stephens, P. J.; Devlin, F. J.; Cheeseman, J. R.; Frisch, M. J. *Chirality* **2002**, *14*, 288. (i) Polavarapu, P. L. *Chirality* **2002**, *14*, 768. (j) Stephens, P. J.; Devlin, F. J.; Cheeseman, J. R.; Frisch, M. J.; Rosini, C. *Org. Lett.* **2002**, *4*, 4595. (k) Stephens, P. J.; Devlin, F. J.; Cheeseman, J. R.; Frisch, M. J.; Bortolini, O.; Besse, P. *Chirality* **2003**, *15*, S57. (l) Stephens, P. J.; McCann, D. M.; Butkus, E.; Stončius, J. R.; Cheeseman, J. R.; Frisch, M. J. *J. Org. Chem.* **2004**, *69*, 1948. (m) Stephens, P. J.; McCann, D. M.; Devlin, F. J.; Cheeseman, J. R.; Frisch, M. J. *J. Am. Chem. Soc.* **2004**, *126*, 7514. (n) Giorgio, E.; Viglione, R. G.; Zanasi, R.; Rosini, C. *J. Am. Chem. Soc.* **2004**, *126*, 12968. (o) McCann, D. M.; Stephens, P. J.; Cheeseman, J. R. *J. Org. Chem.* **2004**, *69*, 8709. (p) Giorgio, E.; Maddau, L.; Spanu, E.; Evidente, A.; Rosini, C. *J. Org. Chem.* **2005**, *70*, 7. (q) Stephens, P. J.; McCann, D. M.; Cheeseman, J. R.; Frisch, M. J. *Chirality* **2005**, *17*, S52. (r) Marchesan, D.; Coriani, S.; Forzato, C.; Pitacco, G.; Ruud, K. *J. Phys. Chem. A* **2005**, *109*, 1449. (s) Giorgio, E.; Roje, M.; Tanaka, K.; Hamersak, Z.; Sunjic, V.; Nakanishi, K.; Rosini, C.; Berova, N. *J. Org. Chem.* **2005**, *70*, 6557. (t) Pecul, M.; Ruud, K. *Adv. Quantum Chem.* **2005**, 50. (u) Crawford, T. D. *Theor. Chem. Acc.* **2006**, *115*, 227. (v) Tam, M. C.; Crawford, T. D. *J. Phys. Chem. A* **2006**, *110*, 2290. (w) Autschbach, J.; Jensen, L.; Schatz, G. C.; Electra Tse, Y. C.; Krykunov, M. *J. Phys. Chem. A* **2006**, *110*, 2461. (x) Kundrat, M. D.; Autschbach, J. *J. Phys. Chem. A* **2006**, *110*, 4115.

(14) (a) Cheeseman, J. R.; Frisch, M. J.; Devlin, F. J.; Stephens, P. J. *Chem. Phys. Lett.* **1996**, *252*, 211. (b) Devlin, F. J.; Stephens, P. J.; Cheeseman, J. R.; Frisch, M. J. *J. Am. Chem. Soc.* **1996**, *118*, 6327. (c) Devlin, F. J.; Stephens, P. J.; Cheeseman, J. R.; Frisch, M. J. *J. Phys. Chem. A* **1997**, *101*, 6322. (d) Devlin, F. J.; Stephens, P. J.; Cheeseman, J. R.; Frisch, M. J. *J. Phys. Chem. A* **1997**, *101*, 9912. (e) Ashvar, C. S.; Devlin, F. J.; Stephens, P. J.; Bak, K. L.; Eggimann, T.; Wieser, H. *J. Phys. Chem. A* **1998**, *102*, 6842. (f) Devlin, F. J.; Stephens, P. J. *J. Am. Chem. Soc.* **1999**, *121*, 7413. (g) Stephens, P. J.; Devlin, F. J. *Chirality* **2000**, *12*, 172. (h) Aamouche, A.; Devlin, F. J.; Stephens, P. J. *J. Am. Chem. Soc.* **2000**, *122*, 2346. (i) Aamouche, A.; Devlin, F. J.; Stephens, P. J. *J. Am. Chem. Soc.* **2000**, *122*, 7358. (j) Aamouche, A.; Devlin, F. J.; Stephens, P. J.; Drabowicz, J.; Bujnicki, B.; Mikolajczyk, M. *Chem.—Eur. J.* **2000**, *6*, 4479. (k) Stephens, P. J. *Encyclopedia of Spectroscopy and Spectrometry*; Academic Press: London, 1999; pp 2415−2421. (l) Stephens, P. J.; Aamouche, A.; Devlin, F. J.; Superchi, S.; Donnoli, M. I.; Rosini, C. *J. Org. Chem.* **2001**, *66*, 3671. (m) Devlin, F. J.; Stephens, P. J.; Scafato, P.; Superchi, S.; Rosini, C. *Tetrahedron: Asymmetry* **2001**, *12*, 1551. (n) Devlin, F. J.; Stephens, P. J.; Scafato, P.; Superchi, S.; Rosini, C. *Chirality* **2002**, *14*, 400. (o) Devlin, F. J.; Stephens, P. J.; Österle, C.; Wiberg, K. B.; Cheeseman, J. R.; Frisch, M. J. *J. Org. Chem.* **2002**, *67*, 8090. (p) Ceré, V.; Peri, F.; Pollicino, S.; Ricci, A.; Devlin, F. J.; Stephens, P. J.; Gasparrini, F.; Rompietti, R.; Villani, C. *J. Org. Chem.* **2005**, *70*, 664. (q) Devlin, F. J.; Stephens, P. J.; Besse, P. *J. Org. Chem.* **2005**, *70*, 2980. (r) Stephens, P. J.; McCann, D. M.; Devlin, F. J.; Flood, T. C.; Butkus, E.; Stončius, S.; Cheeseman, J. R. *J. Org. Chem.* **2005**, *70*, 3903. (s) Urbanová, M.; Setnička, V.; Devlin, F. J.; Stephens, P. J. *J. Am. Chem. Soc.* **2005**, *127*, 6700. (t) Devlin, F. J.; Stephens, P. J.; Besse, P. *Tetrahedron: Asymmetry* **2005**, *16*, 1557. (u) Devlin, F. J.; Stephens, P. J.; Bortolini, O. *Tetrahedron: Asymmetry* **2005**, *16*, 2653. (v) Krohn, K.; Gehle, D.; Dey, S. K.; Nahar, N.; Mosihuzzaman, M.; Sultana, N.; Sohrab, M. H.; Stephens, P. J.; Pan, J.-J.; Sasse, F. *J. Nat. Prod.* **2007**, *70*, 1339. (w) Stephens, P. J.; Pan, J.-J.; Krohn, K. *J. Org. Chem.* **2007**, *72*, 7641. (x) Cedrón, J. C.; Estévez-Braun, A.; Ravelo, Á.G.; Gutiérrez, D.; Flores, N.; Bucio, M. A.; Pérez-Hernández, N.; Joseph-Nathan, P. *Org. Lett.* **2009**, *11*, 1491. (y) Stephens, P. J.; Devlin, F. J.; Pan, J.-J. *Chirality* **2008**, *20*, 643.

SCHEME 2. Synthetic Route to Norcamphor-Derived Furyl Hydroperoxide

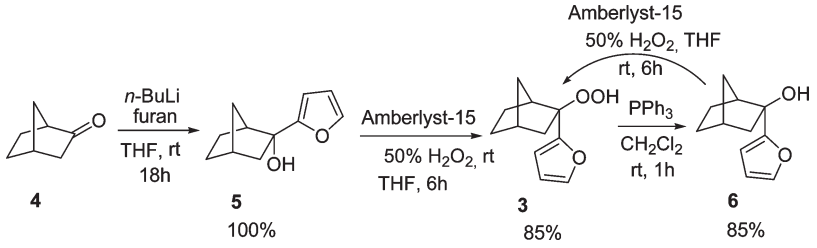

SCHEME 3. Absolute Configurations for Which Optical Rotation and VCD Have Been Calculated

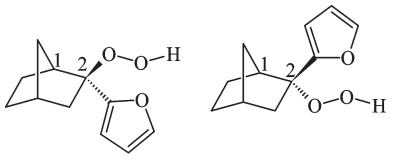

exo-**3** *endo*-**3**

NMR data and the optical rotation of the new alcohol **6** with those of compound **5**. Moreover, in order to confirm that the 2-substituted norbornyl cation intermediate was involved in the reaction, **6** was reacted under the same conditions with hydrogen peroxide. Spectroscopic data and the optical rotation of the hydroperoxide recovered matched those previously determined for compound **3**, thus confirming our hypothesis.

Although the absolute configuration of the newly generated stereogenic carbon at position 2 of the norcamphor skeleton of compound **3** could be guessed, on the basis of literature precedents and experimental findings, a more reliable AC assignment is required. Therefore, the goal of this work is to provide a confident assignment of the absolute configuration of the tertiary hydroperoxide (+)-**3**, thus providing a solid basis for the stereocontrol observed in the synthetic sequence reported in Scheme 2. This has been accomplished using TDDFT calculations of optical rotations[13] and DFT calculations of vibrational circular dichroism (VCD) spectra.[14]

To date, successful examples of the concerted use of transparent spectral region optical rotation and electronic circular dichroism (ECD) have been reported for the AC determination of bicyclo[3.3.1]nonane diones[13l] and [3$_2$]-(1,4)barrelenophanedicarbonitrile.[13m] On the other hand, owing to its high reliability, VCD is frequently used as a stand-alone tool for the configurational and conformational analysis of chiral molecules in solution. A representative set of examples is given in ref 14j,14l−r,t−x. Nevertheless, there are situations where the simultaneous use of more than one chiroptical method is recommended.[15] Our objective here is to find out which of two possible diastereoisomers results from the synthetic route in Scheme 2, i.e., whether (+)-**3** is the *exo* or the *endo* diastereoisomer shown in Scheme 3.

Here, the prefix *exo* or *endo* refers to the orientation of the hydroperoxyl group with respect to the norcamphor bridge, which means that *exo*-**3** corresponds to (1*S*,2*S*,4*R*)-**3** and *endo*-**3** to (1*S*,2*R*,4*R*)-**3**. Since diastereoisomers have independent chiroptical properties, we have used two independent chiroptical methods (OR and VCD) to determine the AC of (+)-**3**.

TABLE 1. Dihedral Angles, Relative Energies, Relative Free Energies, and Percentage Equilibrium Populations of the Most Stable B3LYP/6-31G Conformers of *exo*-3[a]**

conformer	α	β	γ	Δ*E*	Δ*G*	%*P*
a	−144.7	−62.7	−85.9	0.07	0.00	31.2
b	−98.3	169.2	80.6	0.00	0.11	26.1
c	42.7	169.3	85.6	0.58	0.15	24.2
d	62.6	−53.9	−76.6	0.67	0.59	11.5
e	−90.6	171.1	−120.5	1.79	1.49	2.5
f	49.8	172.9	−125.9	2.32	1.70	1.8
g	−86.1	−61.3	109.9	2.36	1.79	1.5
h	34.4	−68.6	107.7	2.23	1.95	1.2

[a]Dihedral angles in degrees are defined as α ≡ C1C2CO, β ≡ C1C2OO and γ ≡ C2OOH; see Scheme 3 for atom numbering. Relative energies and relative free energies in kcal/mol. Percentage equilibrium populations have been computed using relative free energies and Boltzmann statistics at 298 K, including the zero-point energy correction.

For the optical rotation, according to the literature[13h,j,k] and from our previous experience in determining the AC of closely related compounds,[8] a good compromise between accuracy and cost of the calculations can be obtained at the TDDFT/B3LYP level of theory using the polarizability consistent Sadlej (Sadlej-pVTZ) basis set[16] of London's gauge-included atomic orbitals (GIAOs). This choice of basis set might seem unusual, but we should recall that London orbitals, which allow the calculation of origin independent optical rotations, do not guarantee a negligible basis set dependence. One way to reduce the basis set dependence, and also improve the accuracy of the computed optical rotations, is to use a basis set designed to provide optimum molecular electric polarizabilities.[8] The Sadlej-pVTZ basis set is of this type and provides optical rotations as accurate as those obtained by using much larger basis sets.[17] On the other hand, as previously reported,[14j,l−r,t,u] DFT calculations of VCD spectra are best carried out using the B3PW91 and the B3LYP density functionals in conjunction with the TZ2P basis set of GIAOs. Furthermore, since **3** is a highly conformationally flexible molecule, conformational analysis is necessary in order to determine the lowest energy conformers. In the following sections we report OR and VCD predictions based on the specified protocols of calculation, using populations obtained at the B3LYP/6-31G** level, as in ref 8, and the B3PW91/TZ2P and B3LYP/TZ2P levels, as in ref 14j,14l−r,t,u. The concerted

(15) Polavarapu, P. L. *Chirality* **2008**, *20*, 664.

(16) (a) Sadlej, A. J. *Collect. Czech. Chem. Commun.* **1988**, *53*, 1995. (b) Sadlej, A. J. *Theor. Chim. Acta* **1991**, *79*, 123.

(17) Giorgio, E.; Rosini, C.; Viglione, R. G.; Zanasi, R. *Chem. Phys. Lett.* **2003**, *376*, 452.

TABLE 2. Dihedral Angles, Relative Energies, Relative Free Energies, and Percentage Equilibrium Populations Obtained after Reoptimization at the B3PW91/TZ2P and the B3LYP/TZ2P Levels of Theory of the Most Stable Conformers of *exo*-3[a]

	B3PW91/TZ2P						B3LYP/TZ2P					
conformer	α	β	γ	Δ*E*	Δ*G*	%*P*	α	β	γ	Δ*E*	Δ*G*	%*P*
c	49.4	169.6	89.5	0.00	0.00	41.4	49.8	169.6	93.4	0.00	0.00	41.0
a	−149.8	−62.5	−86.9	0.05	0.28	25.8	−150.5	−62.2	−91.0	0.15	0.37	21.9
b	−102.4	170.6	80.7	0.07	0.53	16.9	−101.7	169.7	84.1	0.13	0.57	15.7
d	37.0	−63.7	−94.6	0.76	0.82	10.4	38.5	−62.7	−95.8	0.67	0.63	14.1
f	53.0	174.9	−117.8	1.88	1.78	2.1	51.8	174.8	−121.4	1.73	1.63	2.6
g	−152.4	−66.2	110.9	2.02	2.03	1.3	−153.0	−66.2	114.3	1.95	1.87	1.7
e	−97.4	173.5	−114.5	2.15	2.09	1.2	−94.7	173.0	−117.4	1.87	1.88	1.7
h	36.3	−69.2	105.4	2.13	2.25	0.9	35.9	−69.3	108.4	2.00	2.06	1.3

[a]See Table 1 for definitions.

TABLE 3. Dihedral Angles, Relative Energies, Relative Free Energies, and Percentage Equilibrium Populations of the Most Stable B3LYP/6-31G Conformers of *endo*-3[a]**

conformer	α	β	γ	Δ*E*	Δ*G*	%*P*
a	146.6	59.9	86.7	0.00	0.00	45.6
b	17.3	60.3	82.4	0.34	0.61	16.3
c	−45.8	−171.8	−88.3	1.02	0.61	16.3
d	95.3	−171.6	−80.7	0.43	0.74	13.0
e	157.2	65.2	−115.4	2.04	1.52	3.5
f	44.8	62.4	−117.2	2.16	1.80	2.2
g	84.6	−173.6	118.4	2.19	2.14	1.2
h	−55.0	−176.5	123.4	2.74	2.25	1.0
i	176.9	−163.4	−76.1	1.84	2.31	0.9

[a]See Table 1 for definitions.

application of these two chiroptical techniques will allow us to determine the AC of (+)-**3**.

Methods

1. Experimental Section. Specific rotations of (+)-**3**, obtained according to Scheme 2, have been measured at the sodium D line and room temperature in $CHCl_3$ and hexane solutions of increasing dilution, on a JASCO DIP-1000 digital polarimeter. The IR spectrum of a CCl_4 solution of (+)-**3** at a concentration of 0.15 M was obtained using a Thermo Nicolet Nexus 670 FTIR spectrometer at a resolution of 1 cm^{-1}; the baseline was the solvent spectrum. The VCD spectrum of a CCl_4 solution of (+)-**3** at a concentration of 0.15 M was obtained using a Bomem/BioTools ChiralIR FTIR spectrometer at a resolution of 4 cm^{-1}. The baseline of the VCD spectrum of (+)-**3** was the VCD spectrum of (±)-**3**. A KBr cell of path length 597 μm was used to measure both the IR and VCD spectra.

2. Computational Methods. For both diastereoisomers in Scheme 3 we did the following: (i) conformational analysis with respect to the orientations of the furyl and OOH groups, using the molecular mechanics force field MMFF94 and the Monte Carlo searching method; (ii) geometry reoptimization and vibrational frequency calculation of each of the conformers found in the previous step at the B3LYP /6-31G** level, with the elimination of duplicate conformations and those that were not true potential energy minima, i.e., retaining only those conformers characterized by having all real harmonic vibrational frequencies; (iii) for each of the conformers obtained in step (ii), geometry reoptimization and vibrational frequency calculation at the higher B3PW91/TZ2P and B3LYP/TZ2P levels of theory; then, only for those conformers having a non-negligible population, (iv) TDDFT calculations[13] of the optical rotations at 589.3 nm, using both the B3LYP and the B3PW91 functionals with the Sadlej-pVTZ basis set of GIAOs and using the previously determined optimized geometries and populations; (v) DFT calculations[14] of the IR and VCD spectra using the B3LYP and the B3PW91 functionals in conjunction with the TZ2P basis set of GIAOs. Step (i) was accomplished using Spartan 02,[18] whereas steps (ii)−(v) were carried out using Gaussian 03.[19] Solvent effects were not included in either the geometry optimizations or the chiroptical property calculations.

Results

For conformationally flexibile molecules, the prediction of an observable chiroptical property requires, in general, averaging over the contributions of the populated molecular conformations. Consequently, the AC determination increases in complexity. The computed optical rotation $[\alpha]_\lambda$ at each optical wavelength λ of a flexible molecule[13j,k,m,p,r,s,v] is

$$[\alpha]_\lambda = \sum_i x_i [\alpha]_{\lambda,i}$$

where $[\alpha]_{\lambda,i}$ is the optical rotation for the ith conformation, whose fractional equilibrium population is x_i. Likewise, the computed VCD spectrum (and the IR spectrum as well)[14u,y] is determined as the sum of the individual conformer spectra, each one weighted by the fractional equilibrium population x_i of the corresponding conformer. As a result, the conformationally averaged properties are sensitive to both the accuracy of the calculation for each individual conformation and to the conformer populations.

1. Conformational Analysis. First, consider *exo*-**3**. The Monte Carlo MMFF94 search finds 11 conformers (see Table S1 of the Supporting Information), which are stable with respect to changing both the searching method (Monte Carlo or Systematic) and the starting temperature. All conformations survive the B3LYP/6-31G** geometry reoptimization; however a reordering in terms of relative stability occurs (see Table S2 of the Supporting Information). Relative energy and free energy values (Δ*E* and Δ*G*) are less than

(18) *Spartan 02*; Wavefunction Inc., Irvine, CA.

(19) Frisch, M. J.; Trucks, G. W.; Schlegel, H. B.; Scuseria, G. E.; Robb, M. A.; Cheeseman, J. R. J.; Montgomery, A., Jr.; Vreven, T.; Kudin, K. N.; Burant, J. C.; Millam, J. M.; Iyengar, S. S.; Tomasi, J.; Barone, V.; Mennucci, B.; Cossi, M.; Scalmani, G.; Rega, N.; Petersson, G. A.; Nakatsuji, H.; Hada, M.; Ehara, M.; Toyota, K.; Fukuda, R.; Hasegawa, J.; Ishida, M.; Nakajima, T.; Honda, Y.; Kitao, O.; Nakai, H.; Klene, M.; Li, X.; Knox, J. E.; Hratchian, H. P.; Cross, J. B.; Adamo, C.; Jaramillo, J.; Gomperts, R.; Stratmann, R. E.; Yazyev, O.; Austin, A. J.; Cammi, R.; Pomelli, C.; Ochterski, J. W.; Ayala, P. Y.; Morokuma, K.; Voth, G. A.; Salvador, P.; Dannenberg, J. J.; Zakrzewski, V. G.; Dapprich, S.; Daniels, A. D.; Strain, M. C.; Farkas, O.; Malick, D. K.; Rabuck, A. D.; Raghavachari, K.; Foresman, J. B.; Ortiz, J. V.; Cui, Q.; Baboul, A. G.; Clifford, S.; Cioslowski, J.; Stefanov, B. B.; Liu, G.; Liashenko, A.; Piskorz, P.; Komaromi, I.; Martin, R. L.; Fox, D. J. Keith, T.; Al-Laham, M. A.; Peng, C. Y.; Nanayakkara, A.; Challacombe, M.; Gill, P. M. W.; Johnson, B.; Chen, W.; Wong, M. W.; Gonzalez, C.; Pople, J. A. *Gaussian 03*, Gaussian, Inc., Pittsburgh, PA.

TABLE 4. Dihedral Angles, Relative Energies, Relative Free Energies, And Percentage Equilibrium Populations Obtained after Reoptimization at the B3PW91/TZ2P and the B3LYP/TZ2P Levels of Theory of the Most Stable Conformers of *endo*-3[a]

	B3PW91/TZ2P						B3LYP/TZ2P					
conformer	α	β	γ	ΔE	ΔG	%P	α	β	γ	ΔE	ΔG	%P
a	155.3	59.7	88.0	0.00	0.00	55.7	156.2	59.6	92.9	0.00	0.00	51.6
c	−54.7	−173.1	−91.6	0.89	0.54	22.2	−54.7	−173.1	−95.3	0.90	0.53	21.2
b	14.4	61.2	81.4	0.81	1.08	9.0	14.9	60.4	85.3	0.82	0.89	11.4
d	99.4	−173.4	−79.7	1.01	1.19	7.5	99.3	−172.5	−83.5	1.10	1.08	8.4
e	162.8	66.3	−103.7	1.98	1.69	3.2	162.8	66.2	−109.6	1.87	1.47	4.3
h	−56.4	−179.0	113.9	2.71	2.34	1.1	−56.3	−178.8	118.4	2.59	2.14	1.4
f	30.7	64.4	−102.4	2.82	2.52	0.8	37.4	63.7	−108.7	2.50	2.26	1.1
g	90.5	−176.0	112.4	3.05	2.86	0.5	87.5	−175.4	115.9	2.78	2.61	0.6

[a]See Table 1 for definitions.

TABLE 5. Experimental Specific Rotations at 589.3 nm and Room Temperature (24 °C) of 3 in Chloroform and Hexane Solutions of Increasing Dilution[a]

chloroform	hexane
+36.4 (c = 1.00)	+36.9 (c = 1.00)
+33.5 (c = 0.71)	+36.4 (c = 0.72)
+32.9(c = 0.34)	+36.7 (c = 0.34)
+29.6 (c = 0.10)	+36.7 (c = 0.13)
+29.5 (c = 0)	+36.6 (c = 0)

[a]In degrees$[\mathrm{dm(g/cm^3)}]^{-1}$. Concentration c is given in g/100 mL. The values at infinite dilution (last row) have been obtained by linear extrapolation.

TABLE 6. Optical Rotations in Degrees $[\mathrm{dm(g/cm^3)}]^{-1}$ at 589.3 nm Computed for the Most Populated Conformers of *exo*-3 at their B3LYP/6-31G, B3LYP/TZ2P, and B3PW91/TZ2P Equilibrium Geometries Using Their Free Energy-Based Populations with the Sadlej-pVTZ Basis Set and the Same Functionals**

	B3LYP/Sadlej-pVTZ//B3LYP/6-31G**		B3LYP/Sadlej-pVTZ//B3LYP/TZ2P		B3PW91/Sadlej-pVTZ//B3PW91/TZ2P	
conformer	$[\alpha]_{D,i}$	$x_i[\alpha]_{D,i}$	$[\alpha]_{D,i}$	$x_i[\alpha]_{D,i}$	$[\alpha]_{D,i}$	$x_i[\alpha]_{D,i}$
a	−63.43	−19.82	−49.72	−10.89	−62.75	−16.19
b	24.03	6.28	34.16	5.36	38.71	6.54
c	131.41	31.74	122.73	50.32	122.04	50.52
d	4.58	0.52	−59.16	−8.34	−60.91	−6.33
e	−118.64	−2.99				
f	−17.67	−0.31	−12.87	−0.33	−17.35	−0.36
g	122.26	1.85				
h	100.98	1.18				
	$[\alpha]_D$ =	**18.45**	$[\alpha]_D$ =	**36.12**	$[\alpha]_D$ =	**34.18**

TABLE 7. Optical Rotations in Degrees $[\mathrm{dm(g/cm^3)}]^{-1}$ at 589.3 nm Computed for the Most Populated Conformers of *endo*-3 at Their B3LYP/6-31G, B3LYP/TZ2P, and B3PW91/TZ2P Equilibrium Geometries Using Their Free Energy-Based Populations with the Sadlej-pVTZ Basis Set and the Same Functionals**

	B3LYP/Sadlej-pVTZ//B3LYP/6-31G**		B3LYP/Sadlej-pVTZ//B3LYP/TZ2P		B3PW91/Sadlej-pVTZ//B3PW91/TZ2P	
conformer	$[\alpha]_{D,i}$	$x_i[\alpha]_{D,i}$	$[\alpha]_{D,i}$	$x_i[\alpha]_{D,i}$	$[\alpha]_{D,i}$	$x_i[\alpha]_{D,i}$
a	135.31	61.66	137.32	70.86	142.06	79.13
b	36.09	5.89	40.53	4.62	43.94	3.95
c	−80.01	−13.01	−76.67	−16.25	−86.21	−19.14
d	44.72	5.80	32.94	2.77	25.20	1.89
e	−12.16	−0.43	−8.14	−0.35	−9.85	−0.32
f	−97.14	−2.11				
g	195.55	2.40				
h	55.04	0.56				
i	−43.59	−0.40				
	$[\alpha]_D$ =	**60.36**	$[\alpha]_D$ =	**61.64**	$[\alpha]_D$ =	**65.52**

or close to 2 kcal/mol for a subset comprising the first eight conformations, which have been labeled **a**−**h** according to increasing ΔG. Higher energy conformations have negligible populations and can be ignored. Table 1 summarizes the dihedral angles (α, β, γ), the relative energies (ΔE), the relative free energies (ΔG), and the free energy-based Boltzmann equilibrium populations at 298 K obtained at the B3LYP/6-31G** level. In general, free energy derived populations are different from those obtained from energy alone (see Supporting Information). However, to make a meaningful comparison with experimental data obtained at room temperature, free energy-based populations are to be preferred over those obtained from energy alone, and as a result, the corresponding free energy derived chiroptical properties should be considered to be the final predictions. Free energy-based populations are used in this study. Nevertheless, one should be aware that the free energy calculation is based on a number of further approximations, which could introduce additional errors especially when low frequency vibrational modes are present.

It is interesting to note (see Table S2 of the Supporting Information) that, at this level of theory, conformer **d** has the shortest distance between the H of the hydroperoxide and the O of the furyl group, but it is not the most stable conformer; three other conformers (**a**, **b**, and **c**) with H−O distances outside the range of hydrogen bonding appear to have a lower energy.

The molecular geometries of the eight conformations (**a**−**h**), reported in Table 1, have been reoptimized using the B3PW91 and the B3LYP functionals in conjunction with the larger TZ2P basis set. The results of these higher level calculations are summarized in Table 2.

As can be observed, the two functionals are in good agreement. The largest differences, ∼4°, are in the dihedral angles γ. The population sequence is the same, although the weights of conformers **a**(**d**) are predicted to be larger(smaller) by the B3PW91 and B3LYP functionals, respectively. Conversely, comparing the relative energies, relative free energies, and populations with those obtained using B3LYP/6-31G** (see Table 1), a number of significant differences can be observed. In particular, conformer **c** is now the most stable, with an equilibrium population as large as 41%. The basis set influence on relative free energies and populations is also rather large for conformers **a**, **b**, and **d**. In going from B3LYP/6-31G** to B3LYP/TZ2P the structures of the conformations do not change radically except for conformer

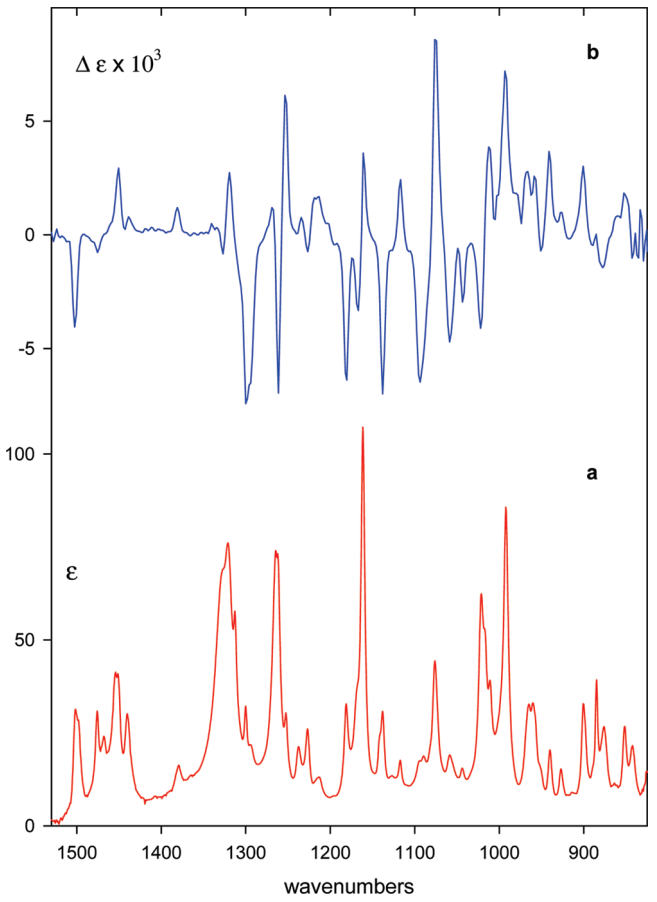

FIGURE 1. (a) IR absorption spectrum of (+)-**3** in CCl_4; 0.15 M, path length 597 μm. (b) VCD spectrum of (+)-**3** in CCl_4; 0.15 M, path length 597 μm.

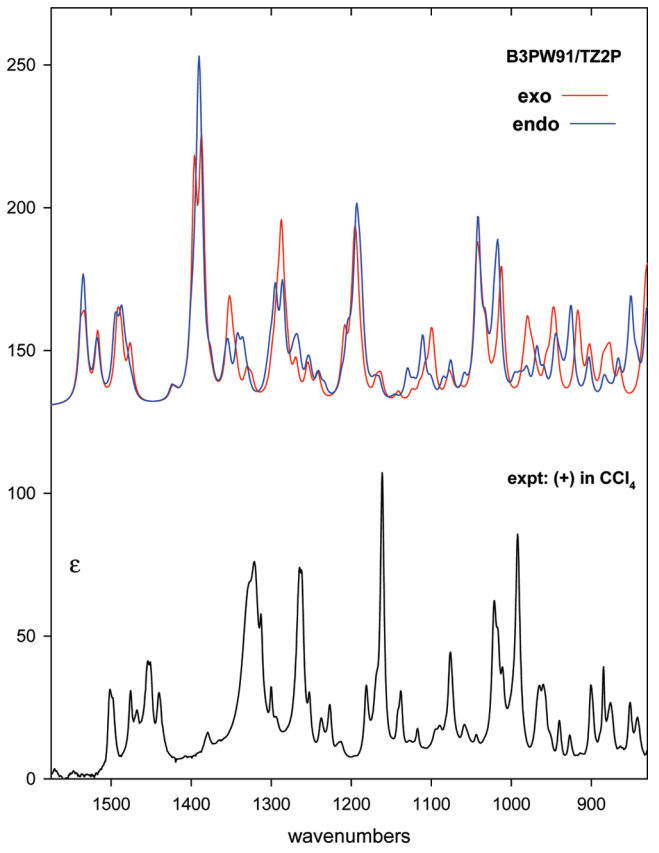

FIGURE 2. Comparison of the conformationally averaged B3PW91/TZ2P IR spectra of *exo*-**3** (red) and *endo*-**3** (blue) to the experimental IR spectrum of (+)-**3**. Room-temperature equilibrium populations were obtained from B3PW91/TZ2P relative free energies (Tables 2 and 4).

d (dihedrals α and γ change by ~24 and ~20°, respectively) and conformer **g** (dihedral α changes by ~60°). As a consequence, rather different chiroptical properties are expected to result from these higher level equilibrium geometries and populations compared to those obtained with the smaller 6-31G** basis set.

Now, consider the other possible diastereoisomer *endo*-**3**. The Monte Carlo MMFF94 search finds 13 conformers (see Table S4 of the Supporting Information). All of them survive the B3LYP/6-31G** geometry reoptimization with some reordering in terms of relative stability (see Table S5 of the Supporting Information). Nine conformers have relative energy values (ΔE and ΔG) less than or close to 2 kcal/mol. They have been labeled from **a** to **i** as ΔG increases. Table 3 summarizes the dihedral angles, the relative energies, the relative free energies, and the room-temperature equilibrium populations obtained at the B3LYP/6-31G** level.

In this case also (see Table S5 of the Supporting Information), the conformer having the shortest distance between the H of the hydroperoxide and the O of the furyl group, namely **i**, is not the most stable conformer.

The molecular geometries of the first eight conformations (**a**−**h**), given in Table 3, have been reoptimized at the B3PW91/TZ2P and the B3LYP/TZ2P levels of theory. The results are summarized in Table 4.

As can be observed, the agreement between the two functionals is rather satisfactory in this case too. The largest difference, ~7°, is in the dihedral angle α of conformer **f**. The population sequence is the same with only minor differences, as, for example, in the case of conformers **a** and **b** whose weights are predicted to be slightly larger and smaller by the B3PW91 and the B3LYP functionals, respectively. In going from B3LYP/6-31G** (see Table 3) to B3LYP/TZ2P conformation **a** remains the most stable with a larger population of 52%, while conformations **b** and **c** are interchanged. Since the structures of the conformations are similar, we do not expect, in this case, large discrepancies in the calculated chiroptical properties on passing from one set of equilibrium geometries and populations to another.

2. Optical Rotation. 2.1. Experimental Section. Specific rotations of **3**, obtained according to Scheme 2, have been measured at the sodium D line and room temperature in $CHCl_3$ and hexane solutions. The results are listed in Table 5.

Intrinsic rotations obtained by extrapolating the specific rotations to infinite dilution are reported in the last row of Table 5. As can be observed, dilution has a measurable effect only for $CHCl_3$ solutions, which is likely to indicate the presence of solute−solute interactions, i.e., aggregation. Since the optical rotation at the highest concentration is very similar for the two solvents, one can suppose that aggregation may also occur in hexane and that it is not removed by dilution in this nonpolar solvent. However, since the variation in OR value is small, this indicates that, apart from aggregation, the solvent has only a moderate effect.

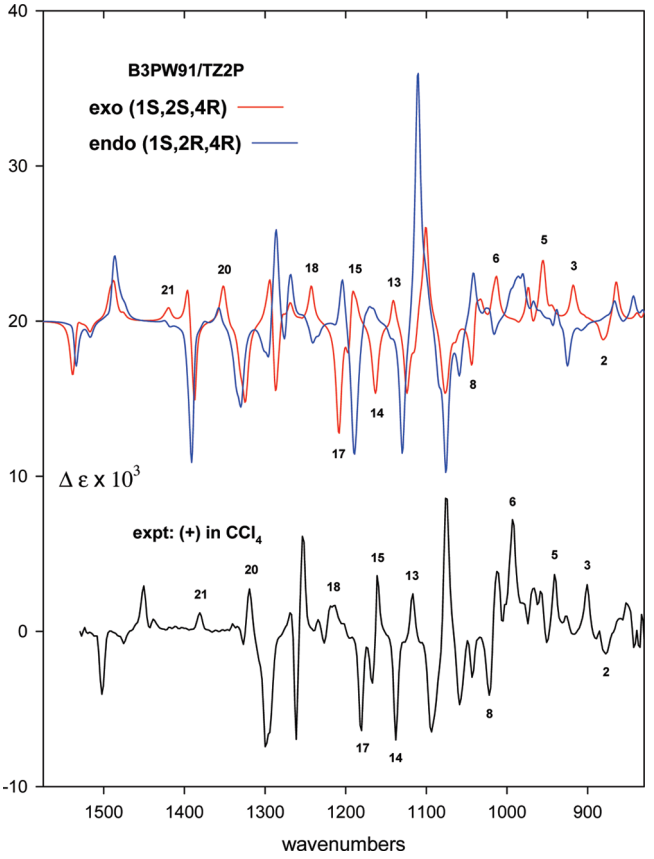

FIGURE 3. Comparison of the conformationally averaged B3PW91/TZ2P VCD spectra of (1*S*,2*S*,4*R*)-**3** (red) and (1*S*,2*R*,4*R*)-**3** (blue) to the experimental VCD spectrum of (+)-**3**. Room-temperature equilibrium populations were obtained from B3PW91/TZ2P relative free energies (Tables 2 and 4). Numbers are attached to bands of *exo*-**3** which differ in sign and/or magnitude from those of *endo*-**3** and which can be assigned to corresponding bands in the experimental VCD spectrum of (+)-**3**.

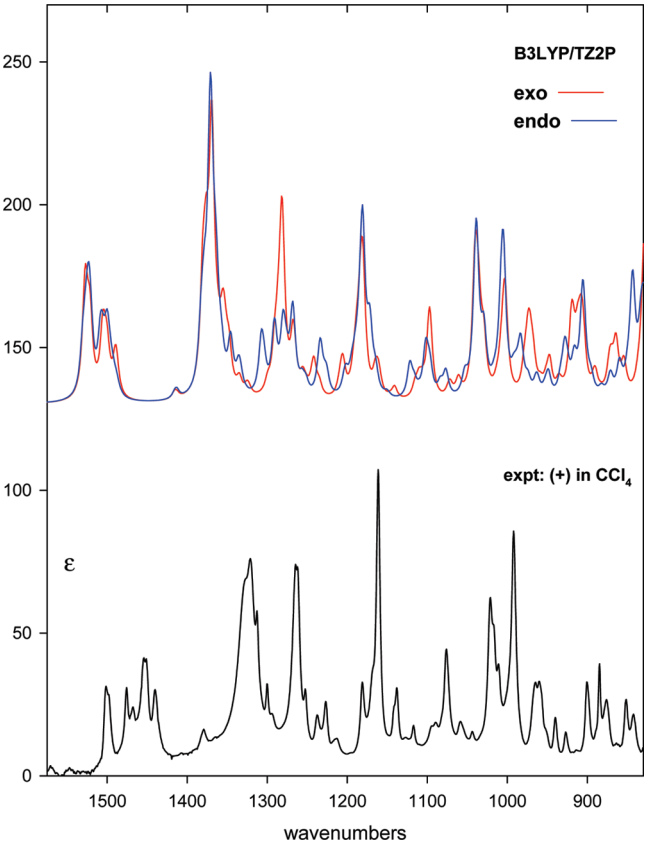

FIGURE 4. Comparison of the conformationally averaged B3LYP/TZ2P IR spectra of *exo*-**3** (red) and *endo*-**3** (blue) to the experimental IR spectrum of (+)-**3**. Room-temperature equilibrium populations were obtained from B3LYP/TZ2P relative free energies (Tables 2 and 4).

2.2. Calculations. The results obtained for *exo*-**3** and *endo*-**3** are summarized in Tables 6 and 7, respectively. Additional details can be found in the Supporting Information. In both tables, the optical rotations at 589.3 nm are calculated for the most populated conformers at their B3LYP/6-31G**, B3PW91/TZ2P, and B3LYP/TZ2P equilibrium geometries. The OR of each individual conformation $[\alpha]_{D,i}$ is reported along with its contribution $x_i\,[\alpha]_{D,i}$ to the averaged optical rotation, where x_i is the free energy-based fractional population of the conformer (see Tables 1−4).

For *exo*-**3**, it can be observed that the B3PW91/Sadlej-pVTZ//B3PW91/TZ2P and the B3LYP/Sadlej-pVTZ//B3LYP/TZ2P rotations are very similar with the exception of conformer **a**, whose optical rotation is ∼13° higher with the B3PW91 functional. In going from B3LYP/Sadlej-pVTZ//B3LYP/6-31G** to B3LYP/Sadlej-pVTZ//B3LYP/TZ2P the optical rotations of the conformations undergo fairly large changes. This is particularly evident for conformer **d**, whose optical rotation changes radically from ∼+4 to ∼−60, as a consequence of the different structure. At all levels, the largest contribution is given by conformer **c**, which is positive, the second important contribution is given by conformer **a**, which is negative, and partially cancels those of **c** and **b**. Since **a** is the most stable conformation at the B3LYP/6-31G** level and **c** is the most stable conformer at the higher B3PW91/TZ2P and B3LYP/TZ2P levels, the cancellation of terms is more effective in the former case. The final computed optical rotations of *exo*-**3** are positive in all cases. In particular, the B3PW91/Sadlej-pVTZ//B3PW91/TZ2P and the B3LYP/Sadlej-pVTZ//B3LYP/TZ2P predictions are in good agreement, being +34.2 and +36.1, respectively. As expected, the B3LYP/Sadlej-pVTZ//B3LYP/6-31G** rotation, +18.5, is significantly different.

For *endo*-**3**, it can be observed that the B3PW91/Sadlej-pVTZ//B3PW91/TZ2P and B3LYP/Sadlej-pVTZ//B3LYP/TZ2P rotations are very similar in this case too, with the exception of conformer **c** whose optical rotation is ∼10° higher with the B3PW91 functional. In going from B3LYP/Sadlej-pVTZ//B3LYP/6-31G** to B3LYP/Sadlej-pVTZ//B3LYP/TZ2P the optical rotations of the conformations undergo only minor changes, with the exception of conformer **d**, whose optical rotation becomes ∼12° smaller, as a consequence of the different structure. At all levels, conformer **a** is the most stable and provides by far the largest contribution to the optical rotation. Conformers **b**−**d** give the only other significant contributions, and since the optical rotation of **c** is negative and those of **b** and **d** are positive, some partial cancellation occurs. As a result of the different populations and individual OR values, conformers **b**−**d** have a net contribution to the optical rotation of −1.3° (B3LYP/Sadlej-pVTZ//B3LYP/6-31G**), −13.3° (B3PW91/Sadlej-pVTZ//B3PW91/TZ2P), and

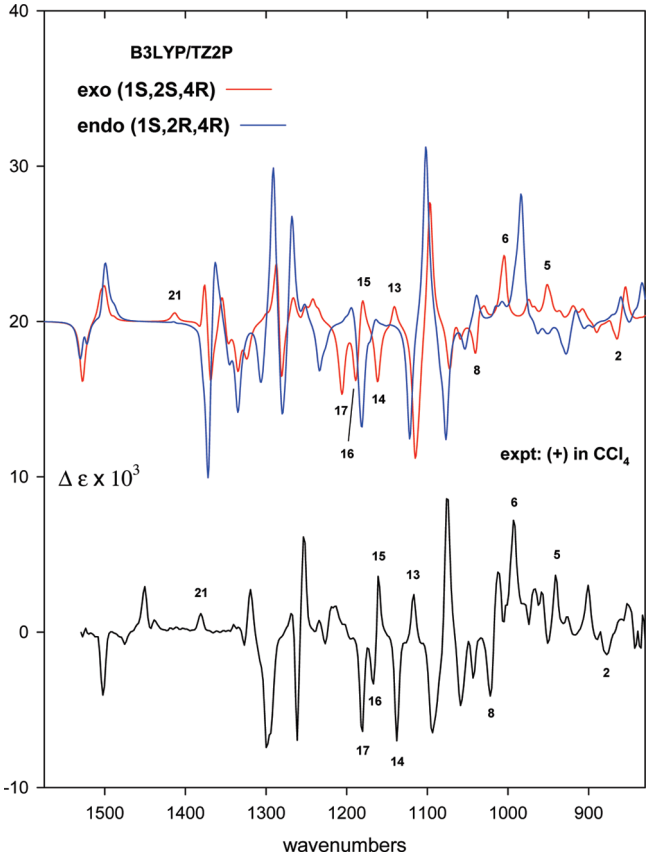

FIGURE 5. Comparison of the conformationally averaged B3LYP/TZ2P VCD spectra of (1*S*,2*S*,4*R*)-**3** (red) and (1*S*,2*R*,4*R*)-**3** (blue) to the experimental VCD spectrum of (+)-**3**. Room-temperature equilibrium populations were obtained from B3LYP/TZ2P relative free energies (Tables 2 and 4). Numbers are attached to bands of *exo*-**3** which differ in sign and/or magnitude from those of *endo*-**3** and which can be assigned to corresponding bands in the experimental VCD spectrum of (+)-**3**.

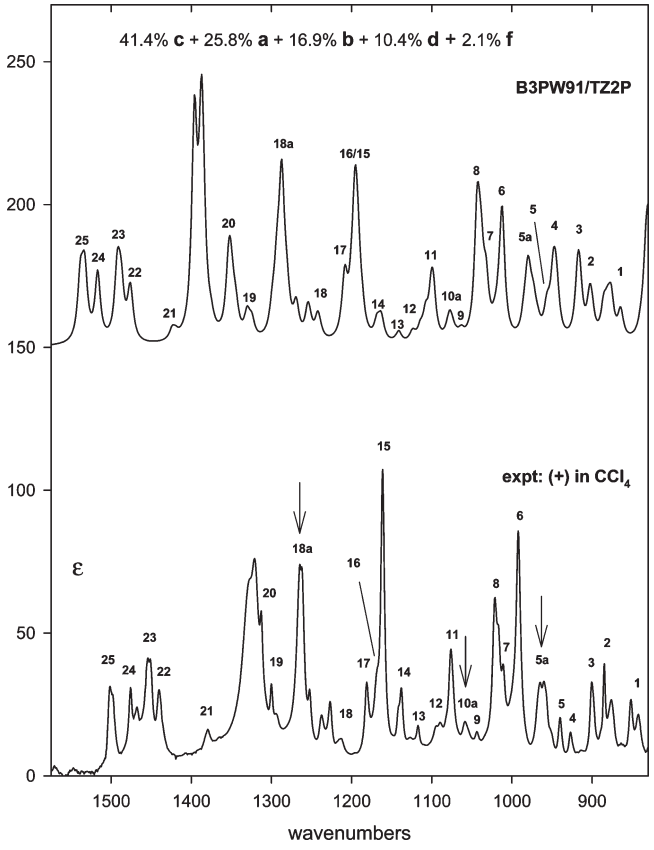

FIGURE 6. Comparison of the conformationally averaged B3PW91/TZ2P IR spectrum of *exo*-**3** to the experimental IR spectrum of (+)-**3**. Fractional equilibrium populations were obtained from B3PW91/TZ2P relative free energies (Table 2). Numbers are attached where the agreement is sufficiently good to assign the experimental bands. Arrows indicate experimental bands due to conformer **a** (see also Figure S1 of the Supporting Information).

−8.9° (B3LYP/Sadlej-pVTZ//B3LYP/TZ2P). The final $[\alpha]_D$ predictions for *endo*-**3** are positive in all cases. The differences in individual contributions are mitigated by the summation and the final rotations are in good agreement, being +60.4°, +65.5°, and +61.6° for B3LYP/Sadlej-pVTZ//B3LYP/6-31G**, B3PW91/Sadlej-pVTZ//B3PW91/TZ2P, and B3LYP/Sadlej-pVTZ//B3LYP/TZ2P, respectively.

By comparing the experimental ORs in Table 5, i.e., +29.5 and +36.6 in $CHCl_3$ and hexane, with the most accurate predictions reported in the last row of Tables 6 and 7, i.e., 34−36 for *exo*-**3** and 62−66 for *endo*-**3**, we can assign the AC of (+)-**3** as being that of *exo*-**3**, i.e., (1*S*,2*S*,4*R*). The optical rotation for *exo*-**3**, obtained with the lower level B3LYP/6-31G** set of geometries and populations, is not sufficiently close to the experimental value to allow a reliable assignment of the AC.

3. Vibrational Circular Dichroism. 3.1. Experimental Section. The IR and VCD spectra of (+)-**3** were measured using a CCl_4 solution of concentration 0.15 M in a cell of path length 597 μm. The baseline for the VCD spectrum of (+)-**3** was the VCD spectrum of (±)-**3**. The IR and VCD spectra in the frequency range 1530−825 cm^{-1} are shown in Figure 1.

3.2. Calculations. In this section we provide a theoretical analysis of the VCD spectrum of (+)-**3**. As a result, the absolute configuration of (+)-**3** will be obtained. The IR spectrum will also be analyzed in order to help assign the experimental bands. The procedure we have followed is a well established one.[14] In particular, the method outlined in ref 14u,14y has been used, according to which, for a conformationally flexible molecule, the computed VCD spectrum (and the IR spectrum as well) is determined as the sum of the individual conformer spectra, each one weighted by the fractional equilibrium population of the corresponding conformer. Obviously, the resulting VCD spectrum is a function of the configuration of the chiral centers, but it also depends on the accuracy of both the calculated rotational strengths of the fundamental vibrational transitions and the predicted populations of the conformers. From previous experience,[14j,l−r,t,u] DFT calculations of VCD spectra are best carried out using the B3PW91 and the B3LYP density functionals in conjunction with the TZ2P basis set of GIAOs for both the rotational strengths and the populations (see Tables 2 and 4 of the conformational analysis section for the latter).

For each conformer of *exo*-**3** and *endo*-**3** having a fractional equilibrium population greater than ~0.015, the IR and VCD spectra have been calculated at both levels of theory. The conformationally averaged IR and VCD spectra of *exo*-**3** and *endo*-**3** are superimposed and displayed in

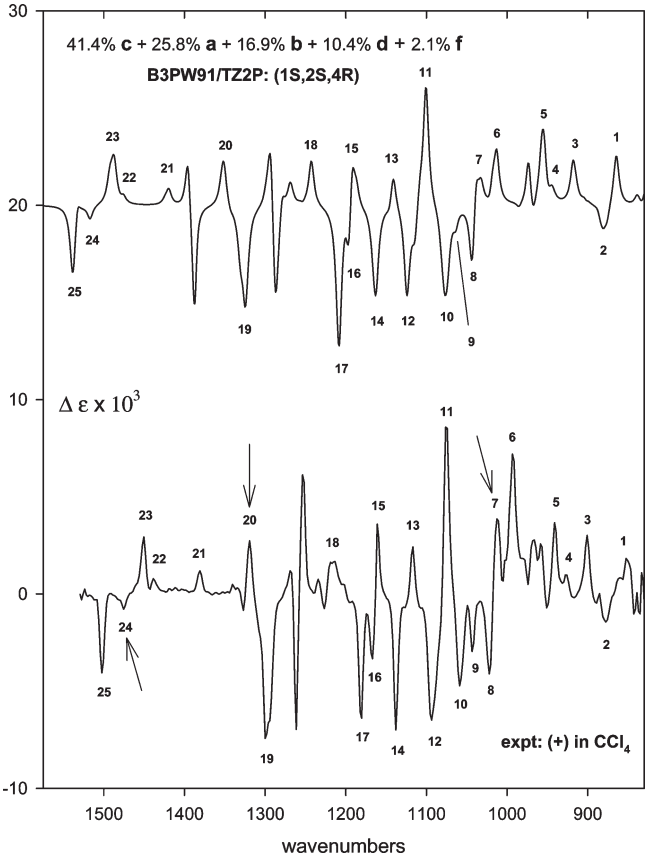

FIGURE 7. Comparison of the conformationally averaged B3PW91/TZ2P VCD spectrum of (1*S*,2*S*,4*R*)-**3** to the experimental VCD spectrum of (+)-**3**. Fractional equilibrium populations were obtained from B3PW91/TZ2P relative free energies (Table 2). Numbers are attached where the agreement is sufficiently good to assign the experimental bands. Arrows indicate experimental bands due to conformer **a** (see also Figure S2 of the Supporting Information).

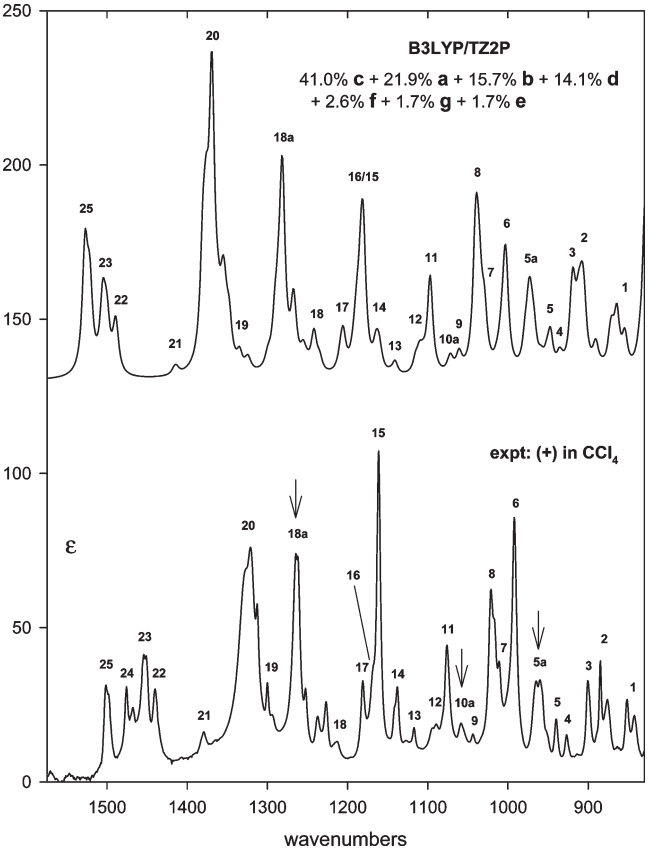

FIGURE 8. Comparison of the conformationally averaged B3LYP/TZ2P IR spectrum of *exo*-**3** to the experimental IR spectrum of (+)-**3**. Fractional equilibrium populations were obtained from B3LYP/TZ2P relative free energies (Table2). Numbers are attached where the agreement is sufficiently good to assign the experimental bands. Arrows indicate experimental bands due to conformer **a** (see also Figure S4 of the Supporting Information).

different colors together with the corresponding experimental spectra in Figures 2−5.

As can be observed, both functionals give results of comparable accuracy overall: in some regions B3PW91 is better and in others B3LYP is better. Although differences between predicted *exo*-**3** and *endo*-**3** IR spectra are not so obvious at both levels of theory, the VCD spectra exhibit a relatively large number of different bands. In particular, differences observed in the B3PW91/TZ2P VCD spectra of Figure 3 are rather significant, as many of the *exo*-**3** bands, which differ from those of *endo*-**3** in sign and/or magnitude, can be found in the experimental VCD spectrum. In Figure 3 numbers have been attached to those characteristic bands of *exo*-**3** which match the experimental ones. As shown in Figure 5, the same is found at the B3LYP/TZ2P level for a slightly lower number of bands. This allows a fairly confident assignment of the AC of (+)-**3** as being that of *exo*-**3**, namely (1*S*,2*S*,4*R*).

Therefore, we can now restrict our attention exclusively to *exo*-**3**, and as shown in Figures 6−9, the calculated IR and VCD spectra of *exo*-**3** enable us to assign most of the experimental bands of (+)-**3**.

Of particular interest is the presence of bands in both the IR and VCD spectra that can be attributed to individual conformations. This occurs when one conformer displays absorptions in regions relatively transparent to all other conformations. In this particular case, band number 10 in the IR spectrum and bands 7 and 20 in the VCD spectrum can be associated with conformer **a** at both levels of theory.

The best assignment of the experimental VCD spectrum of (+)-**3**, based on the DFT calculated VCD spectrum of (1*S*,2*S*,4*R*)-**3**, is shown in Figures 7 and 9. As a result, the AC of **3** is concluded to be (1*S*,2*S*,4*R*)-(+).

Discussion

Unlike enantiomeric pairs, diastereoisomers do not exhibit mirror-image chiroptical properties; consequently, theoretical predictions must be carried out for both of them. Since diastereoisomers have independent chiroptical properties, we have carried out two independent calculations: (i) TDDFT calculation of the optical rotations at 589.3 nm and (ii) DFT calculation of the VCD spectrum. The results have been reported in the previous sections, using a common set of equilibrium geometries and populations and employing computational protocols whose reliability have been assessed in previous studies.[8,14u,14y]

The intrinsic optical rotation at the sodium D line is +29.5 in chloroform and +36.6 in hexane; the most accurate

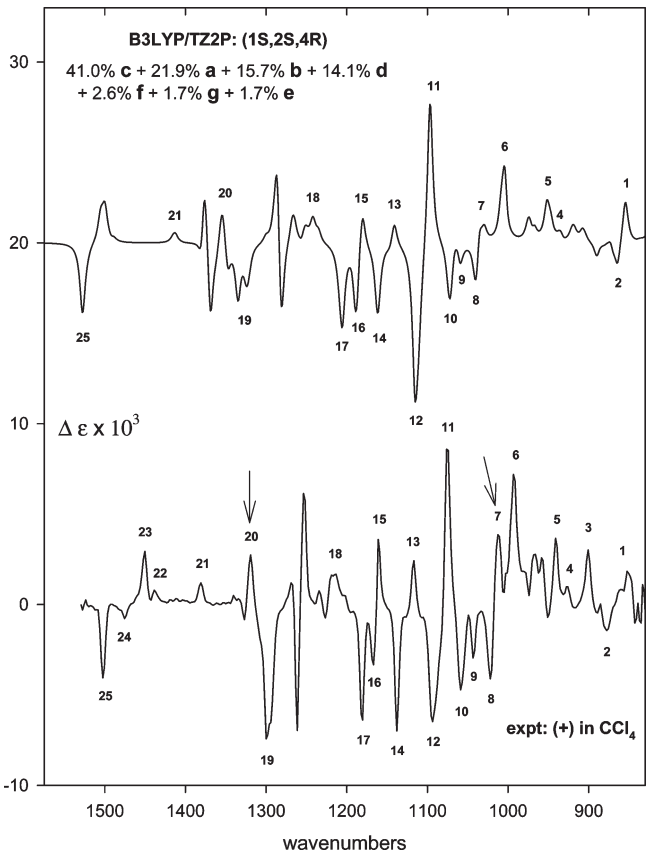

FIGURE 9. Comparison of the conformationally averaged B3LYP/TZ2P VCD spectrum of (1*S*,2*S*,4*R*)-**3** to the experimental VCD spectrum of (+)-**3**. Fractional equilibrium populations were obtained from B3LYP/TZ2P relative free energies (Table 2). Numbers are attached where the agreement is sufficiently good to assign the experimental bands. Arrows indicate experimental bands due to conformer **a** (see also Figure S5 of the Supporting Information).

calculated rotations are in the range +34−36 for *exo*-**3** and +62−66 for *endo*-**3**. The best agreement was obtained for *exo*-**3** using the higher level B3PW91/TZ2P and B3LYP/TZ2P geometries and populations. Quantitatively, the difference between the experimental and calculated rotations lies in the range 0.6−6.5° for *exo*-**3** and 25−36° for *endo*-**3**. This enables us to make an assignment that the absolute configuration of (+)-**3** is that of *exo*-**3**; i.e., (1*S*,2*S*,4*R*). However, we cannot claim that this assignment is 100% reliable, since our conclusion is based on a number of assumptions (for example, choice of calculational method and basis set, neglect of solvent effects and vibrational contributions, and type of populations used) each of which could introduce serious errors. In order to deal with such not easily known effects, a recent investigation,[13q] regarding the reliability of ACs determined by TDDFT calculations for conformationally flexible molecules, has reported a statistically determined error bar of $\pm > 57.8°$. Since this error bar is greater than both of the differences between predicted and experimental optical rotations for *exo*-**3** and *endo*-**3**, our assignment is somewhat unreliable.

A definitive answer is given by the comparison between experimental and computed VCD spectra. VCD spectra have been computed using the same functional and basis set combinations used to obtain the final OR predictions, i.e., B3PW91 and B3LYP in conjunction with the TZ2P basis set of GIAOs. Although the computed IR absorption spectra of *exo*-**3** and *endo*-**3** are practically indistinguishable, the predicted VCD spectra show a number of differences which unequivocally identify the VCD spectrum of (+)-**3** as being that of *exo*-**3**, i.e., (1*S*,2*S*,4*R*)-**3**. Finally, several bands are observed in the experimental IR and VCD spectra which can be assigned to *exo*-**3a**, the second most populated conformer, thus supporting the DFT conformational analysis of **3**.

Particular care must be exercised when calculating equilibrium geometries and populations. As clearly shown here, the B3LYP/6-31G** combination does not provide geometries and populations of sufficient accuracy. Our advice is to use a higher level of theory based on either the B3PW91 or the B3LYP density functional in conjunction with the TZ2P basis set of GIAOs.

Acknowledgment. We are grateful for financial support from the Italian MIUR and the U.S. National Science Foundation (to P.J.S., Grant Nos. CHE-0209957 and CHE-0614577). We also thank the USC High Performance Computing and Communication (HPCC) facility for computer time.

Supporting Information Available: Conformational search details, in terms of dihedral angles, relative energies and relative free energies, and calculated sodium D line specific rotations of *exo*-**3** and *endo*-**3** conformers. Full set of calculated spectra of *exo*-**3** and *endo*-**3** conformers. Full set of B3PW91/TZ2P and B3LYP/TZ2P Cartesian coordinates of conformers **a**−**h** of *exo*-**3** and *endo*-**3**. This material is available free of charge via the Internet at http://pubs.acs.org.